The OsO_4F^-, $OsO_4F_2^{2-}$, and $OsO_3F_3^-$ Anions, Their Study by Vibrational and NMR Spectroscopy and Density Functional Theory Calculations, and the X-ray Crystal Structures of $[N(CH_3)_4][OsO_4F]$ and $[N(CH_3)_4][OsO_3F_3]$

Michael Gerken,[†] David A. Dixon,[‡] and Gary J. Schrobilgen*[,†]

Department of Chemistry, McMaster University, Hamilton, Ontario L8S 4M1, Canada and William R. Wiley Environmental Molecular Sciences Laboratory, Pacific Northwest National Laboratory, 906 Batelle Boulevard, P.O. Box 999, KI-83, Richland, Washington 99352

Received March 7, 2000

The fluoride ion acceptor properties of OsO_4 and OsO_3F_2 were investigated. The salts $[N(CH_3)_4][OsO_4F]$ and $[N(CH_3)_4]_2[OsO_4F_2]$ were prepared by the reactions of OsO_4 with stoichiometric amounts of $[N(CH_3)_4][F]$ in CH_3CN solvent. The salts $[N(CH_3)_4][OsO_3F_3]$ and $[NO][OsO_3F_3]$ were prepared by the reactions of OsO_3F_2 with a stoichiometric amount of $[N(CH_3)_4][F]$ in CH_3CN solvent and with excess NOF, respectively. The OsO_4F^- anion was fully structurally characterized in the solid state by vibrational spectroscopy and by a single-crystal X-ray diffraction study of $[N(CH_3)_4][OsO_4F]$: *Abm*2, $a = 7.017(1)$ Å, $b = 11.401(2)$ Å, $c = 10.925(2)$ Å, $V = 874.1(3)$ Å^3, $Z = 4$, and $R = 0.0282$ at −50 °C. The *cis*-$OsO_4F_2^{2-}$ anion was characterized in the solid state by vibrational spectroscopy, and previous claims regarding the *cis*-$OsO_4F_2^{2-}$ anion are shown to be erroneous. The *fac*-$OsO_3F_3^-$ anion was fully structurally characterized in CH_3CN solution by ^{19}F NMR spectroscopy and in the solid state by vibrational spectroscopy of its $N(CH_3)_4^+$ and NO^+ salts and by a single-crystal X-ray diffraction study of $[N(CH_3)_4][OsO_3F_3]$: *C*2/*c*, $a = 16.347(4)$ Å, $b = 13.475(3)$ Å, $c = 11.436(3)$ Å, $\beta = 134.128(4)°$, $V = 1808.1(7)$ Å^3, $Z = 8$, and $R = 0.0614$ at −117 °C. The geometrical parameters and vibrational frequencies of OsO_4F^-, *cis*-$OsO_4F_2^{2-}$, monomeric OsO_3F_2, and *fac*-$OsO_3F_3^-$ and the fluoride affinities of OsO_4 and monomeric OsO_3F_2 were calculated using density functional theory methods.

Introduction

Osmium tetroxide has been shown to act as a Lewis acid toward a large number of organonitrogen bases,[1−10] forming adducts, which have been characterized by vibrational spectroscopy[2−5] and by single-crystal X-ray diffraction.[5−10] Lewis acid−base adducts of OsO_4 with oxygen donor molecules have been prepared with the bases OH^- [1,11−19] and *N*-methylmorpholine *N*-oxide.[10] Adducts of osmium tetroxide with fluoride[11,13,20−22] and chloride[4] have been reported. The OsO_4Cl^- and $OsO_4N_3^-$ anions were synthesized in CH_2Cl_2 solvent as the PPh_4^+ salts and characterized by infrared spectroscopy, and the OsO_4Cl^- anion has been structurally characterized by X-ray crystallography as the $[PPh_4][OsO_4Cl]$ salt.[4] The *cis*-$OsO_4F_2^{2-}$ anion has reportedly been obtained as its Cs^+ and Rb^+ salts from aqueous solutions,[11,13,20,21] and the vibrational spectra have been interpreted in terms of the cis isomer.[20] In a subsequent study, these workers determined average Os−O and Os−F bond lengths for the compound they formulated as $[Cs]_2$[*cis*-OsO_4F_2] using EXAFS spectroscopy.[22] Adduct formation between OsO_4 and weaker Lewis bases such as OH^- [1,11−19] and (*R*,*R*)-*trans*-1,2-bis(pyrrolidino)cyclohexane[8] was shown to yield hexacoordinate osmium species. Although the composition was not reproducible, it was suggested that the $CsF{\cdot}OsO_4$ adduct, which was obtained from the reaction of CsF and OsO_4 in cold water and was characterized by elemental analyses and vibrational spectroscopy, contained the OsO_4F^- anion.[20]

* To whom correspondence should be addressed.
† McMaster University.
‡ Pacific Northwest National Laboratory.

(1) Fritzmann, E. *Z. Anorg. Allg. Chem.* **1928**, *172*, 213.
(2) Griffith, W. P.; Rossetti, R. *J. Chem. Soc., Dalton Trans.* **1972**, 1449.
(3) Cleare, M. J.; Hydes, P. C.; Griffith, W. P.; Wright, M. J. *J. Chem. Soc., Dalton Trans.* **1977**, 941.
(4) Weber, R.; Dehnicke, K.; Müller, U.; Fenske, D. *Z. Anorg. Allg. Chem.* **1984**, *516*, 214.
(5) Griffith, W. P.; Koh, T. Y.; White, A. J. P.; Williams, D. J. *Polyhedron* **1995**, *14*, 2019.
(6) Griffith, W. P.; Skapski, A. C.; Woode, K. A.; Wright, M. J. *Inorg. Chim. Acta* **1978**, *31*, L413.
(7) Svendsen, J. S.; Markó, I.; Jacobsen, E. N.; Rao, Ch. P.; Bott, S.; Sharpless, K. B. *J. Org. Chem.* **1989**, *54*, 2263.
(8) Corey, E. J.; Sarshar, S.; Azimioara, M. D.; Newbold, R. C.; Noe, M. C. *J. Am. Chem. Soc.* **1996**, *118*, 7851.
(9) Nelson, D. W.; Gypser, A.; Ho, P. T.; Kolb, H. C.; Kondo, T.; Kwong, H.-L.; McGrath, D. V.; Rubin, A. E.; Norrby, P.-O.; Gable, K. P.; Sharpless, K. B. *J. Am. Chem. Soc.* **1997**, *119*, 1840.
(10) Bailey, A. J.; Bhowon, M. G.; Griffith, W. P.; Shoair, A. G. F.; White, A. J. P.; Williams, D. J. *J. Chem. Soc., Dalton Trans.* **1997**, 3245.
(11) Krauss, F.; Wilken, D. *Z. Anorg. Allg. Chem.* **1925**, *145*, 151.
(12) Griffith, W. P. *J. Chem. Soc.* **1964**, 245.
(13) Griffith, W. P. *J. Chem. Soc. A* **1969**, 211.
(14) Nevskii, N. N.; Ivanov-Emin, B. N.; Nevskaya, N. A. *Dokl. Akad. Nauk SSSR* **1982**, *266*, 628.
(15) Nevskii, N. N.; Ivanov-Emin, B. N.; Nevskaya, N. A.; Belov, N. V. *Dokl. Akad. Nauk SSSR* **1982**, *266*, 1138.
(16) Nevskii, N. N.; Porai-Koshits, M. A. *Dokl. Akad. Nauk SSSR* **1983**, *270*, 1392.
(17) Nevskii, N. N.; Porai-Koshits, M. A. *Dokl. Akad. Nauk SSSR* **1983**, *272*, 1123.
(18) Ivanov-Emin, B. N.; Nevskaya, N. A.; Zaitsev, B. E.; Nevskii, N. N.; Izmailovich, A. S. *Russ. J. Inorg. Chem. (Engl. Transl.)* **1984**, *29*, 710; *Zh. Neorg. Khim.* **1984**, *29*, 1241.
(19) Jewiss, H. C.; Levason, W.; Tajik, M.; Webster, M.; Walker, N. P. C. *J. Chem. Soc., Dalton Trans.* **1985**, 199.
(20) Jones, P. J.; Levason, W.; Tajik, M. *J. Fluorine Chem.* **1984**, *25*, 195.
(21) Ivanov-Emin, B. N.; Nevskaya, N. A.; Medvedev, Yu. N.; Zaitsev, B. E.; Lin'ko, I. V. *Russ. J. Inorg. Chem. (Engl. Transl.)* **1986**, *31*, 1088; *Zh. Neorg. Khim.* **1986**, *31*, 1889.
(22) Brewer, S. A.; Brisdon, A. K.; Holloway, J. H.; Hope, E. G.; Levason, W.; Ogden, J. S.; Saad, A. K. *J. Fluorine Chem.* **1993**, *60*, 13.

10.1021/ic000259i CCC: $19.00
Published on Web 08/23/2000

The $OsO_3F_3^-$ anion is better documented and has been synthesized as the $[K][OsO_3F_3]$, $[Cs][OsO_3F_3]$, and $[Ag][OsO_3F_3]$ salts by the reactions of OsO_4 with BrF_3 and KBr, CsBr, and $AgIO_3$, respectively, in excess BrF_3 at room temperature[23] and as the Cs^+, Rb^+, K^+, and Na^+ salts by the reactions of OsO_3F_2 with the corresponding alkali metal fluorides.[20] The facial geometry was suggested for the $OsO_3F_3^-$ anion on the basis of the vibrational spectra of the Cs^+, K^+, Rb^+, and Na^+ salts.[13,20] Bond lengths for the $OsO_3F_3^-$ anion in $[K][OsO_3F_3]$ have been estimated from EXAFS spectroscopy.[22]

The present work was undertaken to reinvestigate the formation and characterization of the OsO_4F^- and $OsO_4F_2^{2-}$ anions, for which there is ambiguous and conflicting evidence in the literature, and provides the first definitive structural studies of the OsO_4F^- and *cis*-$OsO_4F_2^{2-}$ anions in the solid state and establishes that previous reports concerning the $OsO_4F_2^{2-}$ anion are erroneous. The study also provides the first detailed structural study of the *fac*-$OsO_3F_3^-$ anion in the solid state and in solution.

Results and Discussion

The OsO_4F^- and $OsO_4F_2^{2-}$ Anions. (a) Syntheses. The compound $[N(CH_3)_4][OsO_4F]$ was obtained as an orange solid from the reaction of stoichiometric amounts of $[N(CH_3)_4][F]$ and OsO_4 in CH_3CN solution according to eq 1, where RT

$$[N(CH_3)_4][F] + OsO_4 \xrightarrow{CH_3CN,\ RT} [N(CH_3)_4][OsO_4F] \quad (1)$$

denotes room temperature. The reaction of $[N(CH_3)_4][F]$ with OsO_4 was instantaneous and initially yielded a brown $[N(CH_3)_4]_2[OsO_4F_2]$ precipitate (vide infra) in sample regions where local concentrations of $[N(CH_3)_4][F]$ were high but was reversible upon thorough mixing, yielding an orange $[N(CH_3)_4][OsO_4F]$ precipitate. The $[N(CH_3)_4][OsO_4F]$ salt was slightly soluble in CH_3CN at −40 °C, giving an orange solution, whereas no significant solubility was found for $[N(CH_3)_4][OsO_4F]$ in CHF_3 at temperatures as high as 0 °C in a flame-sealed heavy-walled glass tube. Attempts to observe an ^{19}F NMR signal for OsO_4F^- in CH_3CN solvent at −40 °C were unsuccessful, probably due to intermediate intermolecular exchange between the labile fluoride ligand of OsO_4F^- and low concentrations of the free fluoride ion (eq 2). Under these conditions, the ^{19}F NMR signal

$$OsO_4F^- + CH_3CN \rightleftharpoons OsO_4{\cdot}CH_3CN + F^- \quad (2)$$

is likely to be broad and indistinguishable from the baseline. This is consistent with the long Os−F bond observed in OsO_4F^- (see X-ray Crystal Structure of $[N(CH_3)_4][OsO_4F]$) and with the low Os−F stretching frequency observed in the infrared spectrum of OsO_4F^- (see Raman and Infrared Spectroscopy of $[N(CH_3)_4][OsO_4F]$).

The compound, $[N(CH_3)_4]_2[OsO_4F_2]$, was initially obtained in an admixture with $[N(CH_3)_4][OsO_4F]$ and $[N(CH_3)_4][F]$ by reaction of OsO_4 with a stoichiometric amount of $[N(CH_3)_4][F]$ in CH_3CN solution according to eq 3. In CH_3CN solvent,

$$2[N(CH_3)_4][F] + OsO_4 \xrightarrow{CH_3CN,\ -20\ °C} [N(CH_3)_4]_2[OsO_4F_2] \quad (3)$$

$[N(CH_3)_4]_2[OsO_4F_2]$ is dark brown, but it is light brown-ochre when dry. The reaction presumably does not go to completion, because $[N(CH_3)_4][OsO_4F]$ is occluded by $[N(CH_3)_4]_2[OsO_4F_2]$. Repeated washings with CH_3CN at −30 °C produced $[N(CH_3)_4]_2[OsO_4F_2]$ having only a minor amount of $[N(CH_3)_4][OsO_4F]$ impurity.

Table 1. Summary of Crystal Data and Refinement Parameters for $[N(CH_3)_4][OsO_4F]$ and $[N(CH_3)_4][OsO_3F_3]$

	$[N(CH_3)_4][OsO_4F]$	$[N(CH_3)_4][OsO_3F_3]$
space group	*Abm*2 (No. 39)	*C*2/*c* (No. 15)
a (Å)	7.017(1)	16.347(4)
b (Å)	11.401(2)	13.475(3)
c (Å)	10.925(2)	11.436(3)
α (deg)	90	90
β (deg)	90	134.128(4)
γ (deg)	90	90
V (Å^3)	874.1(3)	1808.1(7)
Z (molecules/unit cell)	4	8
mol wt	347.35	369.35
calcd density (g cm^{-3})	2.639	2.714
T (°C)	−50	−117
μ (mm^{-1})	78.9	14.13
wavelength (Å) used for data collection	0.560 86	0.710 73
final agreement factors: R,[a] R_w[b]	0.0282, 0.0748	0.0614, 0.1508

[a] $R = \sum||F_o| - |F_c||/\sum|F_o|$. [b] $R_w = \sum|(|F_o| - |F_c|)w^{1/2}|/\sum(|F_o|w)$.

(b) X-ray Crystal Structure of $[N(CH_3)_4][OsO_4F]$. Details of the data collection and other crystallographic information for $[N(CH_3)_4][OsO_4F]$ are given in Table 1, and important bond lengths and angles are listed in Table 2.

The crystal structure consists of well-separated $N(CH_3)_4^+$ cations and OsO_4F^- anions. The tetrahedral $N(CH_3)_4^+$ cation lies on a C_2 axis, giving rise to two crystallographically independent N−C bond lengths which are equal within experimental error and which have the expected values. The OsO_4F^- anion exhibits a distorted trigonal bipyramidal geometry (C_s point symmetry) (Figure 1) in which Os(1), F(1), O(1), and O(2) lie on a crystallographic mirror plane and the two equatorial oxygens, O(3) and O(3A), are symmetry related. The packing can be viewed as an approximate primitive cubic array of $N(CH_3)_4^+$ cations with OsO_4F^- anions occupying all cubic sites (distorted CsCl structure; Supporting Figure S6). The OsO_4F^- anion exhibits long contacts to four $N(CH_3)_4^+$ cations, forming one face of the cation cube. The equatorial O(3) and O(3A) atoms point toward and the O(1)−Os−F(1) bond angle bends toward this face as a consequence of contacts from the axial O(1) atom and the symmetry-equivalent O(3) and O(3A) atoms of OsO_4F^- to the methyl groups of the $N(CH_3)_4^+$ cations. These O···H_3C contacts range from 2.816(10) to 2.827(16) Å and are significantly shorter than the sum of the CH_3 and O van der Waals radii (3.40 Å).[24] Significantly weaker F···H_3C contacts of 3.280(14) and 3.287(14) Å (van der Waals sum 3.35−3.50 Å)[24,25] also exist in $[N(CH_3)_4][OsO_4F]$. The O···H_3C and F···H_3C contacts result in zigzag layers in the *ab* plane, consisting of alternating $N(CH_3)_4^+$ and OsO_4F^- rows (Supporting Figure S6).

The equatorial Os−O(3)/Os−O(3A) bond lengths (1.711(8) Å/1.711(8) Å) and the axial Os−O(1) bond length (1.715(9) Å) are identical within experimental error and are equal, within 3*σ*, to the mean Os−O bond length determined by EXAFS for $OsO_4F_2^{2-}$ (1.701(2) Å).[22] On the basis of the present study (see Raman and Infrared Spectroscopy of $[N(CH_3)_4][OsO_4F]$ and $[N(CH_3)_4]_2[OsO_4F_2]$), the reported vibrational spectrum of the anion studied by EXAFS has been shown to be that of the

(23) Hepworth, M. A.; Robinson, P. L. *J. Inorg. Nucl. Chem.* **1957**, *4*, 24.
(24) Pauling, L. *The Nature of the Chemical Bond*, 3rd ed.; Cornell University Press: Ithaca, NY, 1960; p 260.
(25) Bondi, A. *J. Phys. Chem.* **1964**, *68*, 441.

Table 2. Experimental Bond Lengths (Å), Bond Angles (deg), and Contacts (Å) in $[N(CH_3)_4][OsO_4F]$ and $[N(CH_3)_4][OsO_3F_3]$ and Calculated Geometries (LDFT Level) for OsO_4F^- and $OsO_3F_3^-$

$[N(CH_3)_4][OsO_4F]$

	expt[a]	calc		expt[a]	calc
Os(1)−F(1)	2.075(9)	2.029	Os(1)−O(1)	1.715(9)	1.755
Os(1)−O(2)	1.674(12)	1.743	Os(1)−O(3)	1.711(8)	1.743
O(1)−Os(1)−F(1)	156.9(4)	180.0	O(1)−Os(1)−O(2)	101.4(5)	97.6
O(1)−Os(1)−O(3)	98.5(4)	97.6	O(2)−Os(1)−O(3)	118.4(4)	118.4
O(3)−Os(1)−O(3A)	115.2(8)	118.4	O(2)−Os(1)−F(1)	101.7(5)	82.5
O(3)−Os(1)−F(1)	70.2(4)	82.5			
N(1)−C(1)	1.484(11)		N(1)−C(2)	1.473(11)	
C(1)−N(1)−C(1A)	109.4(10)		C(1)−N(1)−C(2)	110.7(6)	
C(2)−N(1)−C(2A)	109.6(11)				
O(1)···C(2A)	2.816(10)		O(1)···C(2B)	2.816(10)	
O(3)···C(2D)	2.827(16)		F(1)···C(2)	3.280(14)	
F(1)···C(2C)	3.287(14)				

$[N(CH_3)_4][OsO_3F_3]$

	expt[b]	calc		expt[b]	calc
Os(1)−F(1)	1.97(1)	1.955	Os(1)−F(2)	1.91(1)	1.955
Os(1)−F(3)	1.94(1)	1.955	Os(1)−O(1)	1.70(1)	1.735
Os(1)−O(2)	1.72(1)	1.735	Os(1)−O(3)	1.73(1)	1.735
F(1)−Os(1)−F(2)	80.4(5)	78.9	F(1)−Os(1)−F(3)	79.9(4)	78.9
F(2)−Os(1)−F(3)	80.4(5)	78.9	O(1)−Os(1)−O(2)	102.8(8)	100.7
O(1)−Os(1)−O(3)	101.3(7)	100.7	O(2)−Os(1)−O(3)	101.2(7)	100.7
F(1)−Os(1)−O(1)	87.4(6)	89.1	F(1)−Os(1)−O(2)	87.2(6)	89.1
F(2)−Os(1)−O(1)	87.8(7)	89.1	F(2)−Os(1)−O(3)	89.0(5)	89.1
F(3)−Os(1)−O(2)	86.5(6)	89.1	F(2)−Os(1)−O(3)	89.4(5)	89.1
N(1)−C(1)	1.51(2)		N(1)−C(2)	1.48(2)	
N(2)−C(3)	1.50(2)		N(2)−C(4)	1.49(2)	
C(1)−N(1)−C(1A)	109(2)		C(1)−N(1)−C(2)	110(1)	
C(2)−N(1)−C(2A)	111(2)		C(3)−N(2)−C(3A)	110(2)	
C(3)−N(2)−C(4)	110(1)		C(4)−N(2)−C(4A)	108(2)	

[a] A previous EXAFS spectroscopic study of $[Cs][OsO_4F]$,[22] which had been erroneously identified as $[Cs]_2[OsO_4F_2]$, provides average Os−O and Os−F bond lengths of 1.701(2) and 2.048(29) Å, respectively. [b] A previous EXAFS spectroscopic study of $[K][OsO_3F_3]$[22] provides average Os−O and Os−F bond lengths of 1.698(2) and 1.919(15) Å, respectively.

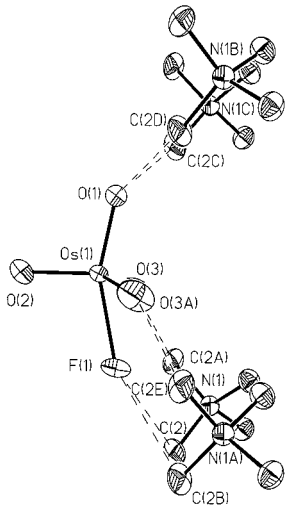

Figure 1. X-ray crystal structure of the OsO_4F^- anion and its contacts with the $N(CH_3)_4^+$ cations in $[N(CH_3)_4][OsO_4F]$. Thermal ellipsoids are shown at the 50% probability level.

OsO_4F^- anion. The Os−O(2) bond length of 1.674(12) Å is significantly shorter than the other Os−O bond lengths and can be explained by packing effects (vide infra). The Os−O(1), Os−O(3), and Os−O(3A) bond lengths are in good agreement with the mean Os−O bond length of 1.713(8) Å reported for OsO_4.[26] The short Os−O(2) bond length is still in the range found for the terminal Os−O bond lengths in the adducts OsO_4·quinuclidine (1.697−1.722 Å)[6] and $OsO_4(OH)OsO_4^-$ (1.62(4)−1.77(3) and 1.64(4)−1.71(3) Å).[19] The contacts from O(1), O(3), O(3A), and F(1) to the $N(CH_3)_4^+$ cations occur on only one side of the cubic hole occupied by the anion (vide supra and Supporting Figure S6), leaving O(2) without long contacts and with less steric crowding, resulting in a significantly shorter Os−O(2) bond. The Os−F bond (2.075(9) Å) in the OsO_4F^- anion is very long compared to the Os−F bonds in *cis*-OsO_2F_4 (1.883(3) and 1.843(3) Å)[27] and the terminal Os−F bond in $(OsO_3F_2)_4$ (1.879(1) Å)[28] but is in excellent agreement with that reported by EXAFS for OsO_4F^- (2.048(29) Å), which has been previously mistaken for the $OsO_4F_2^{2-}$ anion.[22] This bond is, however, considerably shorter than O_4Os−donor atom bonds found in the literature, which range from 2.21(2) Å in $OsO_4(OH)OsO_4^-$ [19] to 2.760(2) Å in OsO_4Cl^-,[4] reflecting the strong Lewis base character of the fluoride ion.

The two crystallographically independent O_{ax}−Os−O_{eq} angles, O(1)−Os−O(2) and O(1)−Os−O(3), are 101.4(5) and 98.5(4)°, respectively. This comparatively small difference in O−Os−O bond angles is in agreement with the O_{ax}−Os−O_{eq} angles found in previously characterized OsO_4 adducts and is reflected in the similarity of the vibrational spectra of the adducts (see Raman and Infrared Spectroscopy of $[N(CH_3)_4][OsO_4F]$), and is indicative of the rigidity of the OsO_4 moiety. Surprisingly, the O(1)−Os−F(1) angle (156.9(4)°) is highly distorted from the O_{ax}−Os−X angle (X = donor atom) found in other Lewis base adducts of OsO_4 where the reported O_{ax}−Os−X angles

(26) Krebs, B.; Hasse, K.-D. *Acta Crystallogr.* **1976**, *B32*, 1334.

(27) Christe, K. O.; Dixon, D. A.; Mack, H. G.; Oberhammer, H.; Pagelot, A.; Sanders, J. C. P.; Schrobilgen, G. J. *J. Am. Chem. Soc.* **1993**, *115*, 11279.

(28) Bougon, R.; Buu, B.; Seppelt, K. *Chem. Ber.* **1993**, *126*, 1331.

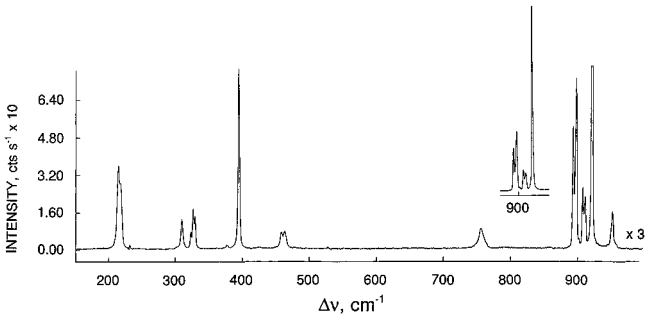

Figure 2. Raman spectrum (low-frequency range) of microcrystalline $[N(CH_3)_4][OsO_4F]$ recorded in a Pyrex capillary at −115 °C using 647.1-nm excitation.

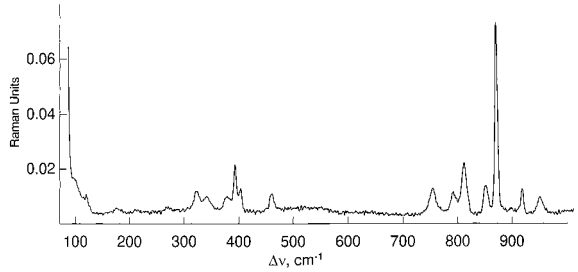

Figure 3. Raman spectrum (low-frequency range) of microcrystalline $[N(CH_3)_4]_2[OsO_4F_2]$ recorded in a Pyrex capillary at −164 °C using 1064-nm excitation.

range from 180.0° in OsO_4·quinuclidine[6] to 175.1(3)° in OsO_4·*N*-methylmorpholine *N*-oxide.[10]

The VSEPR (valence shell electron pair repulsion) model[29] predicts that the most energetically favored geometry for OsO_4F^- is a distorted trigonal bipyramid with one oxygen and the fluorine in the axial positions and the remaining three oxygen atoms in the equatorial positions bent toward the fluorine. This was also the optimized geometry found using local density functional theory (LDFT) calculations (see Computational Results). In the crystal structure of $[N(CH_3)_4][OsO_4F]$, the geometry of the OsO_4F^- anion is, however, found to be a distorted trigonal bipyramid with the fluorine displaced toward one edge of the trigonal plane of the three equatorial oxygens. As a consequence of the rigidity of the OsO_4 moiety, the Os−F bond is quite ionic and can be easily distorted by close contacts with the cations. Because of the greater spatial requirements of Os−O double-bond domains, the OsO_4 unit essentially retains its geometrical integrity with the O_{ax}−Os−F angle distorted by 23.14° from the ideal 180° bond angle of a regular trigonal bipyramid. In light of the computational findings, the distortion of the O_{ax}−Os−F angle is solely attributed to packing and is the consequence of strong O···H_3C contacts and somewhat weaker F···H_3C anion−cation contacts (vide supra).

(c) Raman and Infrared Spectroscopy of $[N(CH_3)_4][OsO_4F]$ and $[N(CH_3)_4]_2[OsO_4F_2]$. The $[N(CH_3)_4][OsO_4F]$ and $[N(CH_3)_4]_2[OsO_4F_2]$ salts were characterized by Raman (Figures 2 and 3) and infrared spectroscopy. The observed vibrational frequencies and their assignments for $[N(CH_3)_4][OsO_4F]$ and $[N(CH_3)_4]_2[OsO_4F_2]$ are given in Tables 3 and 4, respectively. The anion mode assignments are based on LDFT calculations. The $N(CH_3)_4^+$ cation mode assignments are those of Berg[30] and Kabisch[31] and are not further discussed.

The OsO_4F^- anion (C_s point symmetry) possesses 12 fundamental modes of vibration belonging to the irreducible representations 8A′ + 4A″, which are all infrared and Raman active. The room-temperature Raman spectrum of $[N(CH_3)_4][OsO_4F]$ consists of seven bands assigned to OsO_4F^- and those attributed to the $N(CH_3)_4^+$ cation, while several anion bands are split at −115 °C, resulting in 14 anion bands. Correlation of the free anion symmetry to the anion site symmetry (C_s) and the unit cell symmetry (C_{2v}, space group *Abm*2) indicates that the splittings arise from vibrational coupling within the unit cell (factor group splitting; see Supporting Table S8). Only the cation bands $\nu_7(E)$ and $\nu_{19}(T_2)$ are split into three and two components, respectively, in the low-temperature Raman spectrum. No formally inactive bands of the free cation are visible as a result of activity under the factor group.

Three bands in the room-temperature Raman spectrum at 921, 903, and 893 cm^{-1} are assigned to the Os−O stretching modes $\nu_1(A')$, $\nu_2(A')$, and $\nu_3(A')$, respectively. The fourth stretching mode, $\nu_9(A'')$, is presumably hidden under the cation band at 951 cm^{-1}. The Os−O stretches of the adducts OsO_4·1,8-naphthyridine,[5] OsO_4·*N*-methylmorpholine *N*-oxide,[10] and OsO_4·*N*-methylmorpholine[10] were found near 950 cm^{-1} and do not exhibit a strong dependence on the nature of the donor molecule, presumably as a result of the rigidity of the OsO_4 moiety. The strongest Raman band at 921 cm^{-1} corresponds to the totally symmetric stretching mode $\nu_1(A')$, while the bands at 951 and 903 cm^{-1} can be assigned to the asymmetric stretching modes $\nu_9(A'')$ and $\nu_2(A')$, respectively. The band at 893 cm^{-1}, with its intense infrared counterpart, is assigned to the asymmetric stretching mode $\nu_3(A')$. The bands at 903 and 893 cm^{-1} are split into three and two bands, respectively, in the low-temperature Raman spectrum. The splitting of the bands at 903 and 893 cm^{-1} into A_1 and B_1 and into A_2 and B_2 components, respectively, is predicted by the factor group analysis. As expected, the Os−O bonds of the OsO_4F^- anion are more polar and the stretching bands are shifted to lower frequencies relative to those of OsO_4;[32] i.e., the totally symmetric stretch is shifted from 965.2 cm^{-1} ($\nu_1(A_1)$ in OsO_4) to 921 cm^{-1} ($\nu_1(A')$ in OsO_4F^-), while the degeneracy of the asymmetric stretch of OsO_4, $\nu_3(T_2)$, at 960.1 cm^{-1} is removed and the frequencies are shifted to 951, 903, and 893 cm^{-1} for the OsO_4F^- anion. The Os−F stretch is not observed in the Raman spectrum of OsO_4F^-, which is in agreement with the apparent absence of Os−X stretches reported for the Raman spectra of other OsO_4·Lewis base adducts in the literature. However, the strong infrared band at 427 cm^{-1} can be assigned to the Os−F stretching mode, $\nu_4(A')$, and is supported by LDFT calculations (see Computational Results). This frequency is also in accord with the assigned Os−OH stretching frequencies of OsO_4OH^- and $(OsO_4)_2OH^-$, which range from 485 to 490 cm^{-1}.[19] The vibrational bands below 400 cm^{-1} correspond to bending modes, and their assignments are based on density functional theory calculations (see Computational Results).

Two geometries are possible for the $OsO_4F_2^{2-}$ anion, cis and trans. A total of 15 vibrational modes spanning the irreducible representations $6A_1 + 2A_2 + 4B_1 + 3B_2$ under C_{2v} point symmetry (the plane of *cis*-OsF_2 is taken as the *xz* plane) are expected for the cis isomer with all modes Raman active and A_1, B_1, and B_2 infrared active, while 11 vibrational bands belonging to the symmetry species $2A_{1g} + 2A_{2u} + B_{1g} + B_{2g} + B_{2u} + E_g + 3E_u$ are expected for *trans*-$OsO_4F_2^{2-}$ under D_{4h} symmetry with A_{1g}, B_{1g}, B_{2g}, and E_g Raman active and A_{2u} and E_u infrared active. This results in four (Raman and infrared active) and three (mutually exclusive infrared (E_u) and Raman

(29) Gillespie, R. J.; Hargittai, I. *The VSEPR Model of Molecular Geometry*; Allyn and Bacon: Boston, MA, 1991.
(30) Berg, R. W. *Spectrochim. Acta* **1978**, *34A*, 655.
(31) Kabisch, G. *J. Raman Spectrosc.* **1980**, *9*, 279.
(32) Huston, J. L.; Claassen, H. H. *J. Chem. Phys.* **1970**, *52*, 5646.

Table 3. Experimental Vibrational Frequencies and Their Assignments for $[N(CH_3)_4][OsO_4F]$ and Calculated Vibrational Frequencies for OsO_4F^- (C_{3v})

freq,[a] cm^{-1}				
IR[b,c] 25 °C	Raman[d,e] 25 °C	Raman[d,f] −115 °C	calc (LDFT)[g]	assign in C_s [C_{3v}] pt sym for OsO_4F^-
956 vs[h]	951 (13)[h]	954 (7)[h]	918 (372)	$\nu_9(A'')$ [$\nu_5(E)$], $\nu_{as}(OsO_{3eq})$
922 sh	921 (100)	921 (100)	931 (18)	$\nu_1(A')$ [$\nu_1(A_1)$], $\nu_s(OsO_{3eq}) + \nu(OsO_{ax})$
910 sh	903 (19)	912 (10) 908 (11) 902 (2)	918 (372)	$\nu_2(A')$ [$\nu_5(E)$], $\nu_{as}(OsO_{3eq})$
893 vs	893 (40)	898 (32) 893 (23)	893 (167)	$\nu_3(A')$ [$\nu_2(A_1)$], $\nu_s(OsO_{3eq}) - \nu(OsO_{ax})$
858 vw 723 vw				
427 s			471 (49)	$\nu_4(A')$ [$\nu_3(A_1)$], ν(OsF)
394 m*	395 (32)	395 (34)	397 (8)	$\nu_5(A')$ [$\nu_6(E)$], $\delta_{as}(O_{ax}-Os-O_{eq})$
340 m*			397 (8)	$\nu_{10}(A'')$ [$\nu_6(E)$], $\delta_{as}(O_{ax}-Os-O_{eq})$
326 s*	327 (7)	330 (6) 327 (7) 324 (3)	338 (68)	$\nu_6(A')$ [$\nu_4(A_1)$], $\delta_{inv}(OsO_{3eq})$
307 s*	311 (5)	310 (6)	322 (22)	$\nu_7(A')$ [$\nu_7(E)$], $\delta(OsO_{2eq}) + \delta(O_{ax}-Os-O_{eq})$
231 w*		232 (<0.5)	322 (22)	$\nu_{11}(A'')$ [$\nu_7(E)$], $\delta(OsO_{2eq}) + \delta(O_{ax}-Os-O_{eq})$
215 m*	215 (14)	217 (13) 214 (16)	183 (9)	$\nu_8(A')$ [$\nu_8(E)$], $\delta(OsO_{2eq}) - \delta(O_{ax}-Os-O_{eq})$
198 w*			183 (9)	$\nu_{12}(A'')$ [$\nu_8(E)$], $\delta(OsO_{2eq}) - \delta(O_{ax}-Os-O_{eq})$
	83 (1)			lattice mode

[a] Abbreviations denote shoulder (sh), very strong (vs), strong (s), medium (m), weak (w), and very weak (vw). [b] Intensities for the far-IR spectra are denoted by asterisks. [c] The $N(CH_3)_4^+$ cation modes were observed in the infrared spectrum at 373 w*, $\nu_8(E)$; 473 w, $\nu_{19}(T_2)$; 956 vs, $\nu_{18}(T_2)$; 1293 w, $\nu_{17}(T_2)$; 1420 m, $\nu_{16}(T_2)$; 1453 w, $\nu_2(A_1)$; 1494 s, $\nu_6(E)$; and 1699 w, 1802 w, 1829 w, 2171 vw, 2367 w, 2490 w, 2528 w, 2589 w, 2818 w, 2865 w, 2926 w, 2963 w, 3032 m, 3337 vw, 3404 vw, 3492 vw cm^{-1}, ν_{CH_3} and binary bands (see ref 30). [d] Values in parentheses denote relative Raman intensities. [e] The $N(CH_3)_4^+$ cation modes were observed in the Raman spectrum (25 °C) at 462 (6), $\nu_{19}(T_2)$; 756 (10), $\nu_3(A_1)$; 951 (13), $\nu_{18}(T_2)$; 1182 (1), $\nu_7(E)$; 1287 (2), $\nu_{17}(T_2)$; 1416 (5), $\nu_{16}(T_2)$; 1461 (7), $\nu_2(A_1)$; 1475 (9), $\nu_6(E)$; and 2815 (10), 2877 sh, 2893 sh, 2922 (20), 2952 (31), 2982 (16), 3029 (50) cm^{-1}, ν_{CH_3} and binary bands (see ref 30). [f] The $N(CH_3)_4^+$ cation modes were observed in the Raman spectrum (−115 °C) at 379 (1), $\nu_8(E)$; 458 (4), 463 (3), $\nu_{19}(T_2)$; 756 (4), $\nu_3(A_1)$; 954 (7), $\nu_{18}(T_2)$; 1175, 1182, 1188, $\nu_7(E)$; 1290, $\nu_{17}(T_2)$; 1414, $\nu_{16}(T_2)$; 1464, $\nu_2(A_1)$; 1483, $\nu_6(E)$; and 2813, 2963, 3028 cm^{-1}, ν_{CH_3} and binary bands (see ref 30); relative intensities are not reported for the high-frequency bands due to slow decomposition of the sample in the laser beam (647.1-nm line of a Kr^+ laser). [g] Infrared intensities, in km mol^{-1}, are given in parentheses. [h] This band overlaps with $\nu_{18}(T_2)$ of $N(CH_3)_4^+$.

active (A_{1g}, B_{2g})) Os−O stretching bands for *cis*- and *trans*-$OsO_4F_2^{2-}$, respectively. The Raman and infrared spectra of $[N(CH_3)_4]_2[OsO_4F_2]$ show four vibrational bands at 872, 852, 813, and 792 cm^{-1} which are assigned to Os−O stretches and are indicative of the cis arrangement, which was found to be the stable arrangement on the basis of density functional theory calculations (see Computational Results). The preference of the cis isomer over the trans isomer for a pseudooctahedral d^0 transition metal oxide fluoride was previously demonstrated for other dioxo species, e.g., *cis*-OsO_2F_4,[27] *cis*-$ReO_2F_4^-$,[33] and *cis*-$TcO_2F_4^-$ [34] (see X-ray Crystal Structure of $[N(CH_3)_4][OsO_3F_3]$). The Os−O stretching frequencies of *cis*-$OsO_4F_2^{2-}$ reported in the present work occur in the range found for the well-characterized $OsO_4(OH)_2^{2-}$ anion[12,13,18,19] and agree well with those obtained from LDFT calculations. One Os−F stretching band is observed in the Raman spectrum (403 cm^{-1}), while the infrared bands at 428 and 403 cm^{-1} are assigned to the symmetric and asymmetric Os−F stretches which are only 13 and 11 cm^{-1} higher, respectively, than the calculated frequencies. The vibrational bands below 400 cm^{-1} are assigned to bending modes based on LDFT calculations.

The vibrational frequencies obtained for *cis*-$OsO_4F_2^{2-}$ in the present work are in total disagreement with the vibrational frequencies previously reported and assigned to this anion.[13,20] Rather, the previously reported frequencies are shown to belong to the OsO_4F^- anion, and the EXAFS data attributed to $OsO_4F_2^{2-}$ [22] must now be ascribed to the OsO_4F^- anion (see X-ray Crystal Structure of $[N(CH_3)_4][OsO_4F]$).

The $OsO_3F_3^-$ Anion. (a) Syntheses of $[N(CH_3)_4][OsO_3F_3]$ and $[NO][OsO_3F_3]$ and the Solution Characterization of the $OsO_3F_3^-$ Anion by NMR Spectroscopy. Osmium trioxide difluoride reacts with excess NOF over a period of ca. 90 min according to eq 4 to give light orange to ochre $[NO][OsO_3F_3]$

$$NOF + OsO_3F_2 \xrightarrow{\text{NOF, } -78 \text{ to } -60\ ^\circ\text{C}} [NO][OsO_3F_3] \quad (4)$$

at temperatures between −78 and −60 °C. The $[NO][OsO_3F_3]$ salt is insoluble in liquid NOF up to its boiling point (−56 °C) and is unstable at ambient temperature. The compound $[N(CH_3)_4][OsO_3F_3]$ is obtained as a solid orange product by the reaction of stoichiometric amounts of $[N(CH_3)_4][F]$ and OsO_3F_2 in HF solution followed by removal of HF under dynamic vacuum (eq 5). Although OsO_3F_2 is insoluble in anhydrous HF, it rapidly

$$[N(CH_3)_4][F] + OsO_3F_2 \xrightarrow{\text{HF, RT}} [N(CH_3)_4][OsO_3F_3] \quad (5)$$

(33) Casteel, W. J., Jr.; Dixon, D. A.; LeBlond, N.; Lock, P. E.; Mercier, H. P. A.; Schrobilgen, G. J. *Inorg. Chem.* **1999**, *38*, 2340.
(34) Casteel, W. J., Jr.; Dixon, D. A.; LeBlond, N.; Mercier, H. P. A.; Schrobilgen, G. J. *Inorg. Chem.* **1998**, *37*, 340.

Table 4. Experimental Vibrational Frequencies and Their Assignments for $[N(CH_3)_4]_2[OsO_4F_2]$ and Calculated Vibrational Frequencies for *cis*-$OsO_4F_2^{2-}$

freq,[a] cm^{-1}			
IR[c] 25 °C	Raman[d,e] −164 °C	calc (LDFT)[f]	assignt in C_{2v} pt sym[b] for *cis*-$OsO_4F_2^{2-}$
872 s	872 (100)	881 (79)	$\nu_1(A_1)$, $\nu_s(OsO_{2cis}) + \nu_s(OsO_{2trans})$
852 vs	852 (15)	854 (256)	$\nu_9(B_1)$, $\nu_{as}(OsO_{2trans})$
813 vs	813 (27)	842 (342)	$\nu_{13}(B_2)$, $\nu_{as}(OsO_{2cis})$
793 s	792 (12)	833 (121)	$\nu_2(A_1)$, $\nu_s(OsO_{2cis}) - \nu_s(OsO_{2trans})$
774 m			
428 s		415 (50)	$\nu_3(A_1)$, $\nu_s(OsF_2)$
403 s	403 (12)	392 (24)	$\nu_{10}(B_1)$, $\nu_{as}(OsF_2)$
	393 (24)	381 (14)	$\nu_{14}(B_2)$, $\delta_{rock}(OsO_{2trans}$ o.p.$) + \delta_{rock}(OsO_{2cis}$ i.p.$)$
	378 (8)[g]	380 (0)	$\nu_7(A_2)$, $\delta_{rock}(OsO_{2cis}$ o.p.$)$
	340 (8)	355 (41)	$\nu_4(A_1)$, $\delta(OsO_{2trans}$ i.p.$)$
	322 (11)	325 (9)	$\nu_{15}(B_2)$, $\delta_{inv}(F_2OsO_{2trans})$
		301 (88)	$\nu_{11}(B_1)$, $\delta(OsO_{2cis}$ o.p.$) + \delta(O_{trans}-Os-F$ i.p.$)$
	268 (3)	292 (40)	$\nu_5(A_1)$, $\delta(OsO_{2cis}$ i.p.$) + \delta(OsF_2$ i.p.$)$
		239 (0)	$\nu_8(A_2)$, $\delta_{rock}(OsO_{2trans}) + \delta_{rock}(OsF_2$ o.p.$)$
	175 (3)	182 (1)	$\nu_{12}(B_1)$, $\delta(OsO_{2cis}$ o.p.$) - \delta(O_{trans}-Os-F$ i.p.$)$
	119 (6)	122 (1)	$\nu_6(A_1)$, $\delta(OsF_2$ i.p.$) - \delta(OsO_{2cis}$ i.p.$)$
	97 (3)		

[a] Abbreviations denote shoulder (sh), very strong (vs), strong (s), medium (m), weak (w), and very weak (vw). [b] Abbreviations denote in-plane (i.p.) and out-of-plane (o.p.). [c] The $N(CH_3)_4^+$ cation modes were observed in the infrared spectrum at 465 s, $\nu_{19}(T_2)$; 961 vs, $\nu_{18}(T_2)$; 1061 w, 1084 w, 1187 w, 1255 w, 1266 w, 1300 m, $\nu_{17}(T_2)$; 1378 w, 1426 m, $\nu_{16}(T_2)$; 1452 m, 1459 m, $\nu_2(A_1)$; 1498 vs, $\nu_6(E)$; and 1549 w, 1644 w, 1725 w, 1945 w, 2247 w, 2379 w, 2543 w, 2610 w, 2772 w, 2833 w, 2856 w, 2875 w, 2927 m, 2969 m, 3025 s, 3124 w cm^{-1}, ν_{CH_3} and binary bands (see ref 30). Bands associated with the OsO_4F^- impurity were observed in the Raman spectrum at 901 s, $\nu_3(A')$; and 921 w cm^{-1}, $\nu_2(A')$. [d] Values in parentheses denote relative Raman intensities. [e] The $N(CH_3)_4^+$ cation modes were observed in the Raman spectrum (−164 °C) at 378, $\nu_8(E)$; 460 (9), $\nu_{19}(T_2)$; 755 (15), $\nu_3(A_1)$; 953 (9), $\nu_{18}(T_2)$; 1290 (4), $\nu_{17}(T_2)$; 1470 sh (9), 1478 (17), $\nu_2(A_1)$, $\nu_6(E)$; and 2830 (14), 2898 (14) sh, 2923 (23), 2966 (23), 3017 (41) cm^{-1}, ν_{CH_3} and binary bands (see ref 30). Bands associated with an OsO_4F^- impurity were observed in the Raman spectrum at 893 (3), $\nu_3(A')$; and 920 (14) cm^{-1}, $\nu_2(A')$. [f] Infrared intensities, in km mol^{-1}, are given in parentheses. [g] This band overlaps with $\nu_8(E)$ of $N(CH_3)_4^+$.

dissolves in the presence of $[N(CH_3)_4][F]$ to give a pale orange solution of $[N(CH_3)_4][OsO_3F_3]$ at room temperature. The salt has a high solubility in HF even at −78 °C and is moderately soluble in CH_3CN at room temperature.

The ^{19}F NMR spectrum of $[N(CH_3)_4][OsO_3F_3]$ in CH_3CN solvent at −20 °C consists of a singlet at −116.8 ppm ($\Delta\nu_{1/2}$ = 23 Hz) with ^{187}Os ($I = {}^1/_2$, 1.64% natural abundance) satellites which is assigned to the $OsO_3F_3^-$ anion. The magnitude of the coupling ($^1J(^{187}Os-^{19}F) = 32$ Hz) is consistent with those found for *cis*-OsO_2F_4 (35.1 and 59.4 Hz).[27] A broad, weak singlet at −170.0 ppm ($\Delta\nu_{1/2}$ = 125 Hz) indicates the presence of small amounts of HF_2^- exchanging with HF that was not completely removed during the preparation of $[N(CH_3)_4][OsO_3F_3]$. In addition to the HF solvent signal at −194.1 ppm (singlet, $\Delta\nu_{1/2}$ = 10 Hz), the ^{19}F NMR spectrum of $[N(CH_3)_4][OsO_3F_3]$ in HF solvent at −80 °C shows a broad singlet at −164.0 ppm ($\Delta\nu_{1/2}$ = 270 Hz) corresponding to the $OsO_3F_3^-$ anion undergoing slow chemical exchange with HF solvent.

(b) X-ray Crystal Structure of $[N(CH_3)_4][OsO_3F_3]$. Details of the data collection and other crystallographic information for $[N(CH_3)_4][OsO_3F_3]$ are given in Table 1, and important bond lengths and angles are listed in Table 2.

The $N(CH_3)_4^+$ cations pack in an approximate cubic primitive array with the $OsO_3F_3^-$ anions occupying all cubic sites (distorted CsCl structure) (Supporting Figure S7). The anions and cations in the crystal structure are well separated and exhibit only weak contacts between the oxygens and the methyl groups ($O\cdots H_3C$: 3.06(2)−3.36(2) Å) and between the fluorines and the methyl groups ($F\cdots H_3C$: 3.21(2)−3.35(2) Å).

The nitrogen of the $N(CH_3)_4^+$ cation is located on a special position and has an arrangement of carbon atoms that is tetrahedral within experimental error. The bond lengths in both independent cations are the same within experimental error and have the expected values. The environment around the osmium atom is hexacoordinate with Os−O bond lengths (1.70(1)−1.73-(1) Å) significantly shorter than the Os−F bond lengths (1.91-(1)−1.97(1) Å). The oxygen and fluorine atoms exhibit a facial arrangement about Os with O−Os−O bond angles that are considerably larger than 90°, i.e., 102.8(8)−101.2(7)°, and F−Os−F bond angles that are considerably smaller than 90°, i.e., 79.9(4)−80.4(5)° (Figure 4). This is in agreement with the greater repulsion of the Os═O double-bond domains when compared to the Os−F single-bond domains. The Os−O and Os−F bond lengths in $[N(CH_3)_4][OsO_3F_3]$ agree well with those determined by EXAFS for $[K][OsO_3F_3]$, i.e., 1.698(2) and 1.919-(15) Å, respectively.[22] The Os−O bond lengths in $[N(CH_3)_4][OsO_3F_3]$ are larger compared to those of the neutral parent compound, $(OsO_3F_2)_4$, which has a polymeric fluorine-bridged chain structure in the solid state, with Os−O bond lengths of 1.727(1), 1.688(1), and 1.678(1) Å.[28] The terminal Os−F bond length of 1.879(1) Å in $(OsO_3F_2)_4$ is shorter than the Os−F bond lengths in $[N(CH_3)_4][OsO_3F_3]$, which is in accord with the greater polarities of the Os−O and Os−F bonds in the anion.

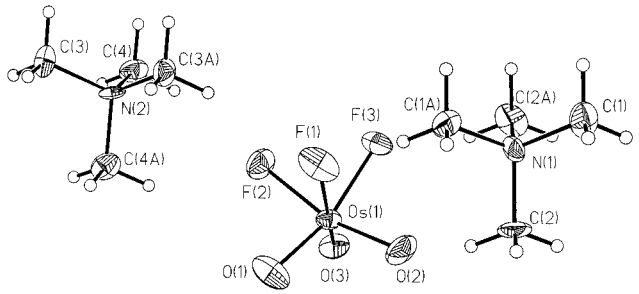

Figure 4. X-ray crystal structures of the *fac*-$OsO_3F_3^-$ anion and the two crystallographically independent $N(CH_3)_4^+$ cations in $[N(CH_3)_4][OsO_3F_3]$. Thermal ellipsoids are shown at the 50% probability level.

The fac isomer of $OsO_3F_3^-$ is expected to be more stable than the mer isomer because each filled p orbital on an oxygen competes for the three available empty $d_{t_{2g}}$ orbitals on the

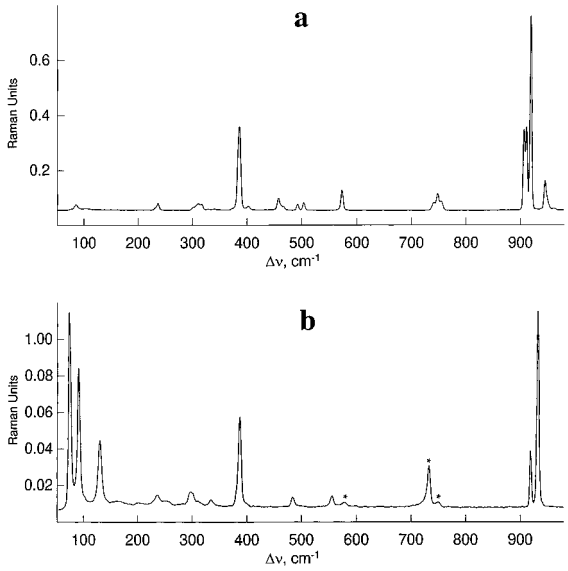

Figure 5. (a) Raman spectrum (low-frequency range) of microcrystalline $[N(CH_3)_4][OsO_3F_3]$ recorded in a Pyrex capillary at −160 °C using 1064-nm excitation. (b) Raman spectrum (low-frequency range) of microcrystalline $[NO][OsO_3F_3]$ recorded in a 4-mm FEP tube at −160 °C using 1064-nm excitation. Asterisks denote the FEP sample tube line.

osmium. An alternative view involves charge concentrations in the outer electron core of osmium located opposite to the doubly bonded oxygens.[35] Additional doubly bonded oxygens avoid the positions of these charge concentrations, disfavoring the *trans*-dioxo and *mer*-trioxo arrangements. Similar arguments have been advanced to account for *cis*-dioxo arrangements (see Raman and Infrared Spectroscopy of $[N(CH_3)_4]_2[OsO_4F_2]$). The preference for the facial arrangement in MO_3F_3 (M = transition metal having a d^0 configuration) moieties has also been demonstrated by the X-ray crystal structures of $[Li]_2[Ta_2O_3F_6]$,[36] $(OsO_3F_2)_4$,[28] $[Ba]_4[Mo_2O_5F_7][HF_2]_3 \cdot H_2O$,[37] and $Pb_5W_3O_9F_{10}$.[38]

(c) Raman and Infrared Spectroscopy of $[N(CH_3)_4][OsO_3F_3]$ and $[NO][OsO_3F_3]$. The $[N(CH_3)_4][OsO_3F_3]$ and $[NO][OsO_3F_3]$ salts were characterized by low-temperature Raman spectroscopy and, in the case of $[N(CH_3)_4][OsO_3F_3]$, by room-temperature infrared spectroscopy. The Raman spectra are shown in Figure 5 and the assignments, made using frequencies calculated from LDFT (see Computational Results), are listed in Table 5.

Assignments for the $OsO_3F_3^-$ anion are based on the facial isomer (C_{3v} point symmetry) as determined by single-crystal X-ray diffraction (see X-ray Crystal Structure of $[N(CH_3)_4][OsO_3F_3]$). The 15 vibrational modes have the symmetries $4A_1 + A_2 + 5E$ with A_1 and E vibrations being Raman and infrared active and the A_2 vibration being inactive. The present assignments for $OsO_3F_3^-$ are in agreement with those previously reported by Griffith,[13] Jeżowska-Trzebiatowska et al.,[39] and Levason et al.,[20] except for $\nu_s(OsO_3)$, which is assigned to bands at 920 ($N(CH_3)_4^+$) and 934 (NO^+) cm^{-1} in the present work. This mode was assigned to an infrared band at 950 cm^{-1} by Griffith and Jeżowska-Trzebiatowska et al. but was not observed in the present work and was suspected by Levason et al. to arise from the hydrolysis product OsO_4. All vibrational modes with E symmetry but one (ν_8) are split into two components in the low-temperature Raman spectrum of $[N(CH_3)_4][OsO_3F_3]$. Correlations of the free anion symmetry with the anion site symmetry (C_1) and the unit cell symmetry (C_{2h}, space group $C2/c$) reveal that these modes are expected to be factor group split (see Supporting Table S9). Fewer bands are split in the low-temperature Raman spectrum of $[NO][OsO_3F_3]$ and may result from a higher site symmetry for the $OsO_3F_3^-$ anion in the crystal lattice of the $[NO][OsO_3F_3]$ salt. While the Os−O stretches appear at lower frequencies in the Raman spectrum of $[N(CH_3)_4][OsO_3F_3]$ than in that of $[NO][OsO_3F_3]$, the opposite trend is observed for the Os−F stretches. This suggests stronger cation···F contacts in the structure of $[NO][OsO_3F_3]$ and is supported by the splitting of the Raman bands associated with fluorine ligand motions.

The Os−O stretches in $OsO_3F_3^-$ anion appear at considerably lower frequencies when compared to those of its neutral parent compound $(OsO_3F_2)_4$,[28] correlating with the longer, more polar Os−O bonds in the anion (see X-ray Crystal Structure of $[N(CH_3)_4][OsO_3F_3]$).

Computational Results

Extensive work in our laboratories has shown that the geometries and vibrational spectra of transition metal oxide fluorides can be predicted reliably at the local density functional theory (LDFT) level. The molecular geometries of the osmium oxide fluorides were optimized at the LDFT level with a polarized double-ζ basis set (DZVP2) and an effective core potential on Os. The calculations were done in the following symmetries: OsO_4, T_d; OsO_4F^-, C_{3v}; $OsO_4F_2^{2-}$, C_{2v} and D_{4h}; OsO_3F_2, D_{3h}; $OsO_3F_3^-$, C_{2v} and C_{3v}.

The calculated values for OsO_4 (Table 6) show that the bond distances are in very good agreement with the average of the experimental ones.[26] The calculated harmonic vibrational frequencies for OsO_4 are in excellent agreement with the experimental values,[32] with the two calculated stretching frequencies being 26 (A) and 22 (T_2) cm^{-1} higher than the experimental anharmonic values. The calculated bending frequencies are also in excellent agreement with the experimental values, the E mode being higher than the T_2 bending mode, just as found experimentally.

Addition of a fluoride ion to OsO_4 yields the OsO_4F^- anion with C_{3v} symmetry (Table 2). The experimental X-ray structure has C_s symmetry due to nonlinearity of the O_{ax}−Os−F_{ax} moiety with an angle of 156.9(4)° (see X-ray Crystal Structure of $[N(CH_3)_4][OsO_4F]$). The calculated geometry has Os−O bond distances that are longer than the experimental ones by 0.044 Å, when compared to the equatorial average, and by 0.040 Å for Os−O_{ax}. This is typical of what is found in other transition metal oxide fluorides where the calculated values are somewhat longer than the experimental ones. The calculated difference between the Os−O_{eq} and Os−O_{ax} bond lengths is 0.012 Å compared to the experimental difference between the average Os−O_{eq} bond lengths and the Os−O_{ax} bond length of 0.016 Å. The calculated Os−O_{eq} bond length in the adduct is 0.025 Å longer than the calculated bond length for OsO_4, consistent with anion formation. The calculated Os−F bond length is shorter than the experimental one by 0.046 Å, suggesting that the charge distribution was not perfectly reproduced by the calculations. A longer Os−F bond is expected to result in shorter Os−O bonds in the experimental structure. The calculated O−Os−O bond angles are in reasonable agreement with the experimental

(35) Gillespie, R. J.; Bytheway, I.; Tang, T.-H.; Bader, R. F. *Inorg. Chem.* **1996**, *35*, 3954.
(36) Kaskel, S.; Strähle, J. *Z. Anorg. Allg. Chem.* **1997**, *623*, 456.
(37) Fourquet, J. L.; Duroy, H.; Crosnier-Lopez, M. P. *Z. Anorg. Allg. Chem.* **1997**, *623*, 439.
(38) Abrahams, S. C.; Marsh, P.; Ravez, J. *J. Chem. Phys.* **1987**, *87*, 6012.
(39) Jeżowska-Trzebiatowska, B.; Hanuza, J.; Bałuka, M. *Acta Phys. Pol.* **1970**, *A38*, 563.

Table 5. Experimental Vibrational Frequencies and Their Assignments for $[N(CH_3)_4][OsO_3F_3]$ and $[NO][OsO_3F_3]$ and Calculated Vibrational Frequencies for *fac*-$OsO_3F_3^-$

freq,[a] cm^{-1}				
$[N(CH_3)_4][OsO_3F_3]$		$[NO][OsO_3F_3]$		
IR[b] 25 °C	Raman[c,d] −160 °C	Raman[c,e] −160 °C	calc (LDFT)[f]	assignt in C_{3v} pt sym for *fac*-$OsO_3F_3^-$
920 m	920 (100)	934 (100)	941 (76)	$\nu_1(A_1)$, $\nu_s(OsO_3)$
909 vs	912 (43) 908 (42)	920 (29)	930 (350)	$\nu_6(E)$, $\nu_{as}(OsO_3)$
609 w				
567 s	573 (11)	555 (6)	599 (128)	$\nu_2(A_1)$, $\nu_s(OsF_3)$
506 s	504 (4)		526 (115)	$\nu_7(E)$, $\nu_{as}(OsF_3)$
494 s	493 (3)	483 (5)		
	402 (2)		374 (8)	$\nu_8(E)$, $\delta_{as}(OsO_3)$
	385 (43)	386 (45)[g]	371 (8)	$\nu_3(A_1)$, $\delta_s(OsO_3)$
	339 (<0.5) 328 (<0.5)	332 (4)	323 (55)	$\nu_9(E)$, $\delta_{as}(OsF_3) + \delta_{as}(F-Os-O)$
	316 (3) 310 (3) 301 (2)	307 (2) 295 (7)[g]	321 (16)	$\nu_4(A_1)$, $\delta_s(OsF_3)$
	235 (3) 230 (1)	249 (2) 234 (5)	233 (3)	$\nu_{10}(E)$, $\delta_{as}(OsF_3)$-$\delta_{as}(F-Os-O)$
			190 (0)	$\nu_5(A_2)$, $\tau(OsF_3)$ wrt OsO_3
	102 (<0.5) 84 (2)	128 (32) 89 (69) 72 (100)		lattice modes

[a] Abbreviations denote shoulder (sh), very strong (vs), strong (s), medium (m), weak (w), very weak (vw). [b] The $N(CH_3)_4^+$ cation modes were observed in the infrared spectrum at 464 w, $\nu_{19}(T_2)$; 953 m, $\nu_{18}(T_2)$; 1291 w, $\nu_{17}(T_2)$; 1381 vw, 1421 w, $\nu_{16}(T_2)$; 1453 w, 1461 m, $\nu_2(A_1)$; 1492 w, $\nu_6(E)$; and 1828 w, 2365 vw, 2856 m, 2926 m, 2957 m, 3041 m cm^{-1}, ν_{CH_3} and binary bands (see ref 30). [c] Values in parentheses denote relative Raman intensities. [d] The $N(CH_3)_4^+$ cation modes were observed in the Raman spectrum (−160 °C) at 457 (6), 467 (2), $\nu_{19}(T_2)$; 742 (2), 749 (9), 756 (5), $\nu_3(A_1)$; 948 (15), 965 (1), $\nu_{18}(T_2)$; 1175 (2), 1181 (2), $\nu_1(E)$; 1290 (2), $\nu_{17}(T_2)$; 1410 sh, 1414 (2), $\nu_{16}(T_2)$; 1445 (<0.5), 1460 (7), $\nu_2(A_1)$; 1472 (9), $\nu_6(E)$; and 1501 (1), 2808 (4), 2816 (4), 2868 (1), 2876 (1), 2889 (3), 2908 (4), 2913 (4), 2922 (7), 2931 (5), 2962 (18), 2979 (6), 2986 (6), 2997 (5), 3002 (5), 3024 (9), 3035 (27), 3046 (10) cm^{-1}, ν_{CH_3} and binary bands (see ref 30). [e] The NO^+ cation mode was observed in the Raman spectrum (−160 °C) at 2319 (37) cm^{-1}, ν(NO). Bands arising from the FEP sample tube were observed at 295 (7), 386 (45), 578 (3), 733 (21), and 750 (3) cm^{-1}. [f] Infrared intensities, in km mol^{-1}, are given in parentheses. [g] This band overlaps with a band arising from the FEP sample tube.

Table 6. Calculated Geometries for OsO_4, OsO_3F_2, and *cis*-$OsO_4F_2^{2-}$ and Vibrational Frequencies (cm^{-1}) for OsO_4 (T_d) and OsO_3F_2 (D_{3h})[a]

OsO_4			OsO_3F_2			$OsO_4F_2^{2-}$	
	calc (LDFT)	expt[b]		calc (LDFT)[c]	expt[d]		calc (LDFT)
d(Os−O)	1.718 Å	1.698 Å 1.727 Å	d(Os−O_{eq}) d(Os−F_{ax})	1.717 Å 1.889 Å		Os−O_{cis} Os−O_{trans} Os−F O_{cis}−Os−O_{cis}	1.780 Å 1.769 Å 2.078 Å 153.1°
$\nu_1(A)$	991	965.2	$\nu_1(A_1')$, $\nu_s(OsO_3)$	970 (0)	946.5	F−Os−F	98.6°
$\nu_2(E)$	338	333.1	$\nu_5(E')$, $\nu_{as}(OsO_3)$	969 (200)	929.0 (928.0)	O_{trans}−Os−O_{trans}	98.6°
$\nu_3(T_2)$	982	960.1	$\nu_3(A_2'')$, $\nu_{as}(OsF_2)$	673 (179)	(646.0)	O_{cis}−Os−O_{trans}	98.7°
$\nu_4(T_2)$	334	322.7	$\nu_2(A_1')$, $\nu_s(OsF_2)$	626 (0)	619.0	O_{cis}−Os−F	80.1°
			$\nu_8(E'')$, δ_{as}(O−Os−F)	352 (0)	348.0	O_{trans}−Os−F	88.3°
			$\nu_6(E')$, $\delta_{as}(OsO_3)+\delta_{as}(OsF_2)$	303 (7)	317.0 (316.0)		
			$\nu_4(A_2')$, $\delta_s(OsO_3)$	262 (60)	(258.0)		
			$\nu_7(E')$, $\delta_{as}(OsO_3)$-$\delta_{as}(OsF_2)$	179 (10)	206.0		

[a] The calculated geometries for OsO_4F^- and $OsO_3F_3^-$ are included in Table 2; the vibrational frequencies for OsO_4F^-, *cis*-$OsO_4F_2^{2-}$, and $OsO_3F_3^-$ are included in Tables 3−5, respectively. [b] Bond lengths for crystalline OsO_4 from ref 26; Raman frequencies for gaseous OsO_4 from ref 32. [c] Infrared intensities, in km mol^{-1}, are given in parentheses. [d] Raman (infrared) frequencies from ref 40.

results, with differences on the order of 4°. The agreement between the calculated and the experimental vibrational frequencies is quite good (Table 3), considering the effects of crystal packing (see X-ray Crystal Structure of $[N(CH_3)_4][OsO_4F]$). The apparent orderings of the symmetric and asymmetric Os−O_{eq} stretches are reversed in the calculations, with the symmetric stretch being higher than the asymmetric stretch. However, the molecule is strongly distorted in the solid state, which leads to breaking of the degeneracy of the antisymmetric vibration, giving $\nu_2(A')$ and $\nu_9(A'')$. The frequency separation is expected to be strongly dependent on the O_{ax}−Os−F angle and likely results in the appearance of the asymmetric stretch, $\nu_9(A'')$, at higher frequency than that of the totally symmetric stretch, $\nu_1(A')$. The average of the $\nu_2(A')$ and $\nu_9(A'')$ stretches (927 cm^{-1}) is close to the calculated value of 918 cm^{-1}. The largest difference between the calculated and experimental vibrational frequencies is for the Os−F stretch, with the experimental value being 44 cm^{-1} lower than the calculated value, which is consistent with the calculated bond length being significantly shorter than the experimental one. The other

difference worth noting is that the calculated lowest energy bend is 25 cm^{-1} below the average experimental value of 207 cm^{-1}.

Addition of a second fluoride ion to OsO_4F^- to form the $OsO_4F_2^{2-}$ anion can lead to two possible structures, a cis isomer (C_{2v}) and a trans isomer (D_{4h}). The D_{4h} structure is not, however, a stable minimum and exhibits one imaginary frequency. It is 23.7 kcal mol^{-1} above the C_{2v} structure at the LDFT level and 20.8 kcal mol^{-1} above at the gradient-corrected level. The C_{2v} structure shows, as expected, longer Os−O bonds than the monoanion (Table 6). The Os−O bond lengths cis to the fluorine (O_{cis}) are longer than those trans to the fluorine (O_{trans}) by 0.011 Å. The Os−F bond lengths are 0.049 Å longer than those in the monoanion. The calculated Os−O stretching frequencies are 2−41 cm^{-1} higher than the experimental values, and the calculated Os−F stretching frequencies are ca. 10 cm^{-1} too low (Table 4). The reported EXAFS data for the $OsO_4F_2^{2-}$ anion[22] match the calculated and observed bond lengths for OsO_4F^- more closely than the calculated bond lengths for $OsO_4F_2^{2-}$ and support our vibrational spectroscopic evidence that the previously claimed preparation of the dianion is erroneous (see Raman and Infrared Spectroscopy of $[N(CH_3)_4]_2[OsO_4F_2]$).

A structure with D_{3h} point symmetry was calculated for monomeric OsO_3F_2 with the oxygen atoms in equatorial positions (Table 6). The Os−O bond lengths are very similar to those in OsO_4. Not unexpectedly, the Os−F bond lengths are significantly shorter than the Os−F bond length in OsO_4F^-. The calculated vibrational frequencies for monomeric OsO_3F_2 are in good agreement with those reported for matrix-isolated OsO_3F_2.[40] The calculated Os−O stretching modes for OsO_3F_2 are 23.5 (A_1') and 30 (E') cm^{-1} higher than the experimental ones and the calculated Os−F stretching frequencies are 27 (A_2'') and 7 (E'') cm^{-1} too low. This trend is also observed for OsO_4 and $OsO_4F_2^{2-}$ (vide infra).

Addition of one F^- to OsO_3F_2 can lead to two possible isomers, a mer isomer (C_{2v}) and a fac isomer (C_{3v}). The mer isomer is not a minimum, having one imaginary frequency and total energies that are 18.7 and 17.5 kcal mol^{-1} above those of the fac isomer at the LDFT and the gradient-corrected DFT levels, respectively. The calculated bond lengths are in good agreement with the experimental values, with the Os−O and Os−F bonds 0.015 and 0.018 Å longer, respectively, than the average experimental values, and the calculated bond angles are within 2° of the average experimental values (Table 2). The calculated stretching frequencies are generally 20 cm^{-1} higher than the experimental values, while most of the calculated bending frequencies are up to 30 cm^{-1} below the observed values, especially for the bends involving the oxygen atoms (Table 5).

The calculated Mulliken charges, Mayer valencies, and Mayer bond orders[41−44] are given in Table 7. A positive charge of 1.69 e is found on the Os atom and negative charges of −0.42 e are found for the O atoms of OsO_4, which are taken as baseline values. The Mayer valencies are 6.14 at Os and 2.26 at O, with a bond order of 1.53. Addition of F^- to form OsO_4F^- leads to a slight decrease in the charge on Os and an increase in the valency at Os. The negative charges on the oxygens increase, and the oxygen valencies and Os−O bond orders decrease. There is a significant negative charge of −0.54 e on the F atom, and the Os−F bond order is 0.55, about one-half of a bond. Addition of a second F^- to form $OsO_4F_2^{2-}$ leads to similar changes. There are a higher positive charge and a slightly higher valency on Os in the OsO_3F_2 monomer than in OsO_4. The valency of O is similar to that in OsO_4, and the Os−O bond order is slightly higher. The Os−F bond order is lower than unity, 0.71. Addition of one F^- leads to the expected charge, valency, and bond order changes.

Table 7. Mulliken Charges, Mayer Valencies, and Mayer Bond Orders for OsO_4, OsO_4F^-, *cis*-$OsO_4F_2^{2-}$, Monomeric OsO_3F_2, and *fac*-$OsO_3F_3^-$

Mulliken Charges

OsO_4		OsO_4F^-		*cis*-$OsO_4F_2^{2-}$		OsO_3F_2		*fac*-$OsO_3F_3^-$	
Os	1.69	Os	1.63	Os	1.54	Os	1.76	Os	1.62
O	−0.42	O_{eq}	−0.52	O_{trans}	−0.60	O	−0.34	O	−0.43
		O_{ax}	−0.52	O_{cis}	−0.60	F	−0.36	F	−0.44
		F_{ax}	−0.54	F	−0.57				

Mayer Valencies

OsO_4		OsO_4F^-		*cis*-$OsO_4F_2^{2-}$		OsO_3F_2		*fac*-$OsO_3F_3^-$	
Os	6.14	Os	6.45	Os	6.73	Os	6.31	Os	6.55
O	2.26	O_{eq}	2.16	O_{trans}	2.07	O	2.31	O	2.24
		O_{ax}	2.15	O_{cis}	2.06	F	1.01	F	0.87
		F_{ax}	0.72	F	0.67				

Mayer Bond Orders

OsO_4		OsO_4F^-		*cis*-$OsO_4F_2^{2-}$		OsO_3F_2		*fac*-$OsO_3F_3^-$	
Os−O	1.53	Os−O_{eq}	1.48	Os−O_{trans}	1.42	Os−O	1.63	Os−O	1.55
		Os−O_{ax}	1.45	Os−O_{cis}	1.41	Os−F	0.71	Os−F	0.63
		Os−F_{ax}	0.55	Os−F	0.53				

The fluoride ion affinities (FA's) of OsO_4 and OsO_3F_2 were calculated at the gradient-corrected DFT level as previously described.[45] FA(OsO_4) was calculated to be 51.2 kcal mol^{-1}, and FA(OsO_3F_2), 80.3 kcal mol^{-1}. The latter is similar to the values of 75.7 and 79.3 kcal mol^{-1} calculated for FA(TcO_2F_3) and FA(ReO_2F_3), respectively.[45] The low fluoride ion affinity of OsO_4 reflects the rigidity of the tetrahedral molecule found by X-ray diffraction and is consistent with the experimentally determined long Os−F bond length and low Os−F stretching frequency.

Conclusions

The X-ray crystal structure of $[N(CH_3)_4][OsO_4F]$ extends the number of structurally well-characterized Lewis acid−base adducts of OsO_4. The OsO_4F^- anion exhibits an unprecedented distortion from trigonal bipyramidal VSEPR geometry with an O_{ax}−Os−F angle of 156.9(4)° instead of the expected 180° angles that are observed in the related OsO_4·Lewis base adducts. The vibrational frequencies assigned to $[N(CH_3)_4]_2[OsO_4F_2]$ are consistent with the cis arrangement for the $OsO_4F_2^{2-}$ anion and are significantly different from those previously reported,[13,20] indicating the presence of the OsO_4F^- anion in the previously reported Lewis acid-base adducts of OsO_4 with the fluoride ion. The single-crystal X-ray structure of $[N(CH_3)_4][OsO_3F_3]$ represents only the second X-ray structure containing an isolated $MO_3F_3^{n-}$ anion (M = d^0 transition metal), the first being that of $WO_3F_3^{3-}$,[38] and unambiguously confirms the facial geometry of the $OsO_3F_3^-$ anion, which was also established in solution by ^{19}F NMR spectroscopy. The geometries and vibrational frequencies of the OsO_4F^-, *cis*-$OsO_4F_2^{2-}$, and *fac*-$OsO_3F_3^-$ anions were calculated at the LDFT level and agree well with the experimental values, except for those of the nonlinear O_{ax}−Os−F arrangement in OsO_4F^-, which can be attributed to the

(40) Beattie, I. R.; Blayden, H. E.; Crocombe, R. A.; Jones, P. J.; Ogden, J. S. *J. Raman Spectrosc.* **1976**, *4*, 313.
(41) Mayer, I. *Chem. Phys. Lett.* **1983**, *97*, 270.
(42) Mayer, I. *Theor. Chim. Acta* **1985**, *67*, 315.
(43) Mayer, I. *Int. J. Quantum Chem.* **1986**, *29*, 73.
(44) Mayer, I. *Int. J. Quantum Chem.* **1986**, *29*, 477.
(45) Casteel, W. J., Jr.; Kolb, P.; LeBlond, N.; Mercier, H. P. A.; Schrobilgen, G. J. *Inorg. Chem.* **1996**, *35*, 929.

occurrence of strong anion−cation contacts in the crystal structure of $[N(CH_3)_4][OsO_4F]$. The fluorine affinities of OsO_4 and monomeric OsO_3F_2 were also calculated and provide the fluoride ion acceptor strength order $OsO_3F_2 > OsO_4$.

Experimental Section

Apparatus and Materials. Volatile materials were handled on vacuum lines constructed of nickel, stainless steel, FEP, and Pyrex, and nonvolatile materials were handled in the atmosphere of a drybox as previously described.[45] Unless indicated otherwise, all syntheses and crystal-growing procedures were carried out in $^1/_4$-in. FEP tubes outfitted with Kel-F valves that had been previously vacuum-dried and passivated with fluorine gas. ***Caution!*** Anhydrous HF and NOF must be handled using appropriate protective gear with immediate access to proper treatment procedures in the event of contact with the liquid or the vapor of either reagent.

Anhydrous $[N(CH_3)_4][F]$,[46] OsO_3F_2,[28] and NOF[47] were prepared by standard literature methods. Osmium tetroxide (Aldrich, 99.8%) was used without further purification. Acetonitrile (HPLC grade, Caledon Laboratories Ltd.)[48] and HF (Harshaw Chemical Co.)[49] were dried and purified by the standard literature methods.

Synthesis of $[N(CH_3)_4][OsO_4F]$. Anhydrous CH_3CN (0.95 mL) was condensed into a tube containing 0.2293 g (0.9021 mmol) of OsO_4 at −196 °C. The OsO_4 dissolved upon warming the mixture to room temperature to give a pale yellow solution to which, after transferring to a drybox and cooling to −110 °C, a stoichiometric amount of $[N(CH_3)_4][F]$ (0.0858 g, 0.9212 mmol) was added. When this mixture was thawed and warmed to −20 °C outside the drybox, a red-brown precipitate formed at the $[N(CH_3)_4][F]-OsO_4/CH_3CN$ solution interface. Mixing at room temperature resulted in the red-brown precipitate merging with the yellow OsO_4/CH_3CN solution to produce a homogeneous orange precipitate. Removal of CH_3CN under dynamic vacuum at room temperature yielded a very finely divided orange powder.

Synthesis of $[N(CH_3)_4]_2[OsO_4F_2]$. Approximately 0.4 mL of anhydrous CH_3CN was condensed onto 0.1642 g (0.6460 mmol) of OsO_4 at −196 °C, and the mixture was warmed to room temperature to effect dissolution, followed by refreezing. Approximately 2 equiv of $[N(CH_3)_4][F]$ (0.1219 g (1.3087 mmol)) was added to the frozen OsO_4/CH_3CN mixture at −110 °C as described in the preceding section. When the resulting mixture was warmed to −25 °C, a red-brown precipitate formed at the $[N(CH_3)_4][F]-OsO_4/CH_3CN$ solution interface, which, when agitated, yielded a homogeneous, brown precipitate. The solvent was removed under dynamic vacuum at −20 °C, followed by pumping at ambient temperature to give 0.2645 g of a light brown-ochre powder. Raman spectroscopy revealed the presence of a mixture of $[N(CH_3)_4]_2[OsO_4F_2]$, $[N(CH_3)_4][OsO_4F]$, and $[N(CH_3)_4][F]$. The product mixture (0.2289 g) was loaded into one arm of a two-arm (h-shaped) Pyrex glass vessel equipped with a 4-mm J. Young Teflon/glass stopcock, and approximately 1.2 mL of CH_3CN was condensed onto the mixture at −196 °C. The resulting mixture was washed 12 times at −30 °C by decanting the faint yellow solution together with some suspended material into the second arm of the vessel at −30 °C, followed by back-distillation of the CH_3CN onto the brown mixture under static vacuum. After removal of CH_3CN, 0.1818 g (80%) of an ochre material was recovered, which, according to its Raman spectrum, still contained significant amounts of $[N(CH_3)_4][OsO_4F]$. Thirteen additional washings were performed on 0.1727 g of material between −25 and −30 °C, yielding 0.1205 g (70%) of ochre $[N(CH_3)_4]_2[OsO_4F_2]$ with only a minor $[N(CH_3)_4][OsO_4F]$ impurity. The $[N(CH_3)_4]_2[OsO_4F_2]$ salt was found to be a significantly weaker Raman scatterer and to be more prone to decomposition in the laser beam (1064-nm excitation) than $[N(CH_3)_4][OsO_4F]$.

Synthesis of $[N(CH_3)_4][OsO_3F_3]$. Approximately 0.4 mL of anhydrous HF was condensed onto 0.1005 g (0.364 mmol) of OsO_3F_2 at −196 °C. When the mixture was warmed to room temperature, OsO_3F_2 was found to be insoluble in HF. Addition of $[N(CH_3)_4][F]$ (0.0342 g, 0.367 mmol) to the refrozen OsO_3F_2/HF mixture at −110 °C, followed by warming to room temperature and mixing, resulted in a clear orange solution. Removal of HF solvent under dynamic vacuum at −78 °C yielded 0.1299 g (0.3517 mmol; 97% yield) of an orange powder. Samples for NMR spectroscopy were prepared from 0.0487 g (0.1319 mmol) [0.0191 g (0.0517 mmol)] of the orange powder and 0.2 [0.2] mL of CH_3CN [HF] solvent in 4-mm FEP tubes, resulting in a yellow-orange supernate and an orange precipitate [a clear yellow solution].

Synthesis of $[NO][OsO_3F_3]$. Approximately 0.04 mL of NOF was condensed into a 4-mm FEP reaction tube containing 0.0500 g (0.181 mmol) of OsO_3F_2 at −196 °C, and the mixture was warmed to −78 °C and agitated for ca. 90 min. Removal of excess NOF at −78 °C yielded a light orange-ochre solid, which was found to decompose upon warming to room temperature.

Growth of $[N(CH_3)_4][OsO_4F]$ Crystals. Sufficient CH_3CN (0.76 mL) was distilled onto 0.0483 g (0.1768 mmol) of $[N(CH_3)_4][OsO_4F]$ to solubilize the solid at 40 °C. Large orange plate-shaped crystals were grown by placing the FEP tube inside a closed dewar of water at 40 °C and allowing the tube contents to cool to ambient temperature over a period of 5 days. The supernate was carefully pipetted off the sample inside a glovebag purged with dry N_2, and residual CH_3CN was removed by rapid evacuation at room temperature for ca. 30 s. The tube containing the crystals was transferred to a drybox, equipped with a microscope, where the crystals were removed and mounted inside 0.5-mm-i.d. Lindemann capillaries, which were then heat sealed. The crystal used for X-ray data collection had the dimensions $0.400 \times 0.442 \times 0.0084$ mm^3.

X-ray Structure Determination of $[N(CH_3)_4][OsO_4F]$. (a) Collection and Reduction of the X-ray Data. A $[N(CH_3)_4][OsO_4F]$ crystal was centered on a Syntex P3 diffractometer using silver radiation monochromatized with a graphite crystal ($\lambda = 0.560\,86$ Å). Accurate cell dimensions were determined at $T = -50$ °C from a least-squares refinement of the setting angles (χ, ϕ, and 2θ) obtained from 29 accurately centered reflections (with $15.32° \le 2\theta \le 32.25°$) chosen from a variety of points in reciprocal space. Integrated diffraction intensities were collected using a $\theta-2\theta$ scan technique with scan rates varying from 1.5 to 14.65°/min (in 2θ) and a scan range of ±0.50° so that the weaker reflections were examined most slowly to minimize counting errors. The data were collected with $-1 \le h \le 11$, $-18 \le k \le 18$, $-14 \le l \le 18$, and $3° \le 2\theta \le 55°$. During data collection, the intensities of three standard reflections were monitored every 97 reflections to check for crystal stability and alignment. Over the course of the data collection, no decay was observed. A total of 6409 reflections were collected, of which 204 were standard reflections. A total of 1214 unique reflections remained after averaging of equivalent reflections, of which 1214 satisfied the condition $I \ge 2\sigma(I)$ and were used for structure solution. Corrections were made for Lorentz and polarization effects. Empirical absorption corrections were applied using the ψ-scan method ($\Delta\phi = 10°$; 001).

(b) Solution and Refinement of the Structure. The XPREP program[50] was used to confirm the unit cell dimensions and the crystal lattice. A solution was obtained using direct methods, which located the position of the osmium atom. Successive difference Fourier syntheses revealed all remaining non-hydrogen atoms, while the positions of the hydrogen atoms were calculated (d(C−H) = 0.97 Å; U_{iso}(H) fixed to $1.5U_{eq}$(C)). It was possible to distinguish four bond lengths in the osmium environment that were significantly shorter than a fifth bond length, indicating the presence of four Os−O double bonds and one long Os−F bond. The final refinement was obtained by introducing a weighting factor ($w = 1/[\sigma^2(F_o^2) + 0.0344^2 + 04.94]$) and anisotropic thermal parameters for all non-hydrogen atoms and gave a residual, R, of 0.0282 (Rw = 0.0748). In the final difference Fourier map, the maximum and minimum electron densities were 2.08

(46) Christe, K. O.; Wilson, W. W.; Wilson, R. D.; Bau, R.; Feng, J. *J. Am. Chem. Soc.* **1990**, *112*, 7619.
(47) Christe, K. O.; Wilson, R. D.; Goldberg, I. B. *Inorg. Chem.* **1976**, *15*, 1271.
(48) Winfield, J. M. *J. Fluorine Chem.* **1984**, *25*, 91.
(49) Emara, A. A. A.; Schrobilgen, G. J. *Inorg. Chem.* **1992**, *31*, 1323.
(50) Sheldrick, G. M. *SHELXTL-Plus*, Release 5.03; Siemens Analytical X-ray Instruments, Inc.: Madison, WI, 1994.

and −1.46 e Å^{-3}, the residual electron density being located around the osmium atom.

All calculations were performed on a Silicon Graphics, Inc., model 4600PC workstation using the SHELXTL-Plus package[50] for the structure determination and refinement and for the molecular graphics.

Growth of $[N(CH_3)_4][OsO_3F_3]$ Crystals. Approximately 0.57 mL of CH_3CN was condensed onto 0.0034 g (0.0123 mmol) of $[N(CH_3)_4][OsO_3F_3]$ at −196 °C. Warming the mixture to 0 °C yielded a clear orange solution. Removal of the CH_3CN solvent from the tube at 0 °C over a period of ca. 1 h yielded thin orange plates as a coating on the walls of the FEP sample tube. Just prior to mounting, the crystals were freed from the walls of the cold vessel by mechanical shocking. The cold sample tube was then cut open under a dry nitrogen stream, and the crystals were immediately dumped onto an aluminum tray cooled by a dry nitrogen cold stream in close proximity to the X-ray diffractometer. A stereomicroscope, positioned above the aluminum tray, was used to select a crystal of appropriate size in the cold stream. The crystal was mounted on a glass fiber by rapidly bringing it into contact with a droplet of Fomblin oil adhering to the tip of the fiber. Upon adhesion of the crystal and solidification of the oil, the crystal was rapidly transferred to the cold stream of the goniometer head. The crystal used in this study had the dimensions 0.30 × 0.15 × 0.01 mm^3.

X-ray Structure Determination of $[N(CH_3)_4][OsO_3F_3]$. (a) Collection and Reduction of the X-ray Data. The X-ray diffraction data for $[N(CH_3)_4][OsO_3F_3]$ were collected using a P4 Siemens diffractometer, equipped with a Siemens SMART 1K charge-coupled device (CCD) area detector (using the program SMART)[51] and a rotating anode and using graphite-monochromated Mo Kα radiation (λ = 0.710 73 Å). The crystal-to-detector distance was 3.991 cm, and the data collection was carried out in a 512 × 512 pixel mode using 2 × 2 pixel binning. A complete sphere of data was collected, to better than 0.8 Å resolution. Processing was carried out by using the program SAINT,[51] which applied Lorentz and polarization corrections to three-dimensionally integrated diffraction spots. The program SADABS[52] was used for the scaling of diffraction data, the application of a decay correction, and an empirical absorption correction based on redundant reflections.

(b) Solution and Refinement of the Structure. The XPREP program[50] was used to confirm the unit cell dimensions and the crystal lattice. A solution was obtained using direct methods, which located the position of the osmium atom. Successive difference Fourier syntheses revealed all remaining non-hydrogen atoms, while the positions of the hydrogen atoms were calculated (d(C−H) = 0.98 Å; U_{iso}(H) fixed to 1.5U_{eq}(C)). The oxygen and fluorine atoms were assigned on the basis of their bond lengths with osmium. The final refinement was obtained by introducing a weighting factor ($w = 1/[\sigma^2(F_o^2) + 0.0839^2]$) and anisotropic thermal parameters for all non-hydrogen atoms, giving a residual, R, of 0.0614 (Rw = 0.1508). In the final difference Fourier map, the maximum and minimum electron densities were 3.68 and −3.92 e Å^{-3}, the residual electron density being located around the osmium atom.

All calculations were performed on a Silicon Graphics, Inc., model 4600PC workstation using the SHELXTL-Plus package[50] for the structure determination and refinement and for the molecular graphics.

Raman Spectroscopy. A sample of $[N(CH_3)_4][OsO_4F]$ at −115 °C in sealed Pyrex melting point capillary was excited with the 647.1-nm line of a Kr ion laser (Lexel Laser, Inc., model 3550), and the Raman spectrum was recorded on a Jobin-Yvon Mole S-3000 triple-spectrograph system as previously described.[45] The spectrum was recorded with a resolution of 1 cm^{-1} and a total of 10 reads, each having a 30 s integration time. The flame-sealed Pyrex melting point capillary containing the sample was placed in a low-temperature microchamber mounted on the microscope stage where dry N_2 gas, chilled by passing through liquid nitrogen, was allowed to flow along the external walls of the capillary. The temperature was measured using a copper−constantan thermocouple (error ±0.8 °C).

The room-temperature Raman spectrum of $[N(CH_3)_4][OsO_4F]$ and the low-temperature Raman spectra of $[N(CH_3)_4]_2[OsO_4F_2]$ (−164 °C; parameters are given in square brackets), $[N(CH_3)_4][OsO_3F_3]$ (−160 °C), and $[NO][OsO_3F_3]$ (−160 °C) were recorded on a Bruker RFS 100 FT Raman spectrometer equipped with a quartz beam splitter, a liquid-nitrogen-cooled Ge diode detector, and a low-temperature accessory. The backscattered (180°) radiation was sampled. The scanner velocity was 5 kHz, and the wavelength range for acquisition was 5500−10 500 [5894−10 394] cm^{-1} when shifted relative to the laser line at 9394 cm^{-1}, giving a spectral range of 3895 to −1105 [3501 to −999] cm^{-1}. The actual usable Stokes range was 50−3500 cm^{-1} with a spectral resolution of 2 [1] cm^{-1}. The Fourier transformations were carried out by using a Blackman−Harris four-term apodization and a zero-filling factor of 4 [2]. The 1064-nm line of an Nd:YAG laser (350 [400] mW maximum output) was used for excitation of the sample with a laser spot of ca. 0.2 mm [<0.1 mm] at the sample. The spectrum of $[N(CH_3)_4][OsO_4F]$ was recorded at ambient temperature for a powdered sample in a thin-walled 5-mm NMR tube using a laser power of 90 mW and a total of 200 scans. The low-temperature spectra of $[N(CH_3)_4]_2[OsO_4F_2]$, $[N(CH_3)_4][OsO_3F_3]$, and $[NO][OsO_3F_3]$ were recorded for powdered samples in melting point capillaries and a 4-mm FEP tube (NO^+ salt) using laser powers of 200, 200, and 300 mW and totals of 1000, 200, and 500 scans, respectively.

Infrared Spectroscopy. FT-infrared spectra were recorded on a Bio-Rad FTS-40 spectrometer at ambient temperature for samples in AgCl disks and for powders in sealed polyethylene bags for regular and far-infrared acquisitions, respectively. The polyethylene bags were filled with $[N(CH_3)_4][OsO_4F]$ powders and temporarily sealed with Kel-F grease inside the drybox before they were heat-sealed outside the drybox. Silver chloride (Alfa, Premion, 99.999%) pellets were made in three layers from vacuum-dried AgCl using a Wilks minipress inside the drybox. The middle layer of an AgCl sample mixture was hermetically sealed by the two outer AgCl layers. The spectra each consisted of 64 scans acquired with a resolution of ±2 cm^{-1} and a 5 kHz scan speed, and the background, which was simultaneously subtracted, was recorded prior to a spectral acquisition. A 6-μm Mylar beam splitter was used for the far-infrared spectrum (170−400 cm^{-1}).

Nuclear Magnetic Resonance Spectroscopy. The ^{19}F NMR spectra (282.409 MHz) of $[N(CH_3)_4][OsO_3F_3]$ were recorded unlocked (field drift <0.1 Hz h^{-1}) on a Bruker AC-300 (7.046 T) spectrometer equipped with an Aspect 3000 computer using a 5-mm ^{1}H/^{13}C/^{19}F/^{31}P combination probe. The spectra were acquired in a 64K/32K memory with a spectral setting of 50 kHz, yielding an acquisition time of 0.654/0.328 s and data point resolution of 1.526/3.052 Hz/data point; a pulse width of 3 μs was used.

Calculations. All calculations were performed with the density functional theory[53] program DGauss[54−56] (DGauss is a density functional program which is part of UniChem and is available from Oxford Molecular; Version 4.1 and 5.0 Beta were used) on SGI computer systems. The Hay−Wadt relativistic ECP and basis sets were used[57−59] with the fitting sets in UniChem for Os[60] and the DZVP2 basis set[61] for O and F. All calculations were done at the local level with the potential fit of Vosko, Wilk, and Nusair.[62] The geometries were optimized by using analytic gradient methods, and second derivatives were also calculated analytically.[63] Single-point gradient-corrected

(51) *SMART* and *SAINT*, Release 4.05; Siemens Energy and Automation Inc.: Madison, WI, 1996.
(52) Sheldrick, G. M. SADABS (Siemens Area Detector Absorption Corrections). Personal communication, 1996.
(53) Parr, R. G.; Yang, W. *Density-Functional Theory of Atoms and Molecules*; Oxford University Press: New York, 1989.
(54) Andzelm, J.; Wimmer, E.; Salahub, D. R. In *The Challenge of d and f Electrons: Theory and Computation*; Salahub, D. R., Zerner, M. C., Eds.; ACS Symposium Series 394; American Chemical Society: Washington, DC, 1989; p 228.
(55) Andzelm, J. In *Density Functional Theory in Chemistry*; Labanowski, J., Andzelm, J., Eds.; Springer-Verlag: New York, 1991; p 155.
(56) Andzelm, J.; Wimmer, E. *J. Chem. Phys.* **1992**, *96*, 1280.
(57) Hay, P. J.; Wadt, W. R. *J. Chem. Phys.* **1985**, *82*, 270.
(58) Hay, P. J.; Wadt, W. R. *J. Chem. Phys.* **1985**, *82*, 284.
(59) Hay, P. J.; Wadt, W. R. *J. Chem. Phys.* **1985**, *82*, 299.
(60) Lee, C.; Chen, H. Unpublished results; see the UniChem Manual, Version 3.0.
(61) Godbout, N.; Salahub, D. R.; Andzelm, J.; Wimmer, E. *Can. J. Chem.* **1992**, *70*, 560.
(62) Vosko, S. H.; Wilk, L.; Nusair, M. *Can. J. Phys.* **1980**, *58*, 1200.

calculations were performed with Becke's exchange functional[64−66] and Perdew's correlation functional.[67] No scaling of the calculated vibrational frequencies was applied.

Acknowledgment. We thank the donors of the Petroleum Research Fund, administered by the American Chemical Society, for support of this work under Grant ACS-PRF No. 33594-AC3. This research was performed in part at the Molecular Science Computing Facility (MSCF), William R. Wiley Environmental Molecular Sciences Laboratory, Pacific Northwest National Laboratory. The MSCF is funded by the Office of Biological and Environmental Research, U.S. Department of Energy. Pacific Northwest National Laboratory is operated by Battelle for the U.S. Department of Energy under Contract DE-AC06-76RLO 1830. We thank the Ontario Ministry of Education and the Richard Fuller and James A. Morrison Memorial Funds for the award of graduate scholarships to M.G. and the Canada Council for the award of a Killam Research Fellowship (1998 and 1999) to G.J.S. We also thank Ms. Barbara A. Fir for assistance with the preparation and characterization of $[N(CH_3)_4][OsO_4F]$.

(63) Komornicki, A.; Fitzgerald, G. *J. Chem. Phys.* **1993**, *98*, 1398 and references therein.
(64) Becke, A. D. *Phys. Rev. A* **1988**, *38*, 3098.
(65) Becke, A. D. In *The Challenge of d and f Electrons: Theory and Computation*; Salahub, D. R., Zerner, M. C., Eds.; ACS Symposium Series 394; American Chemical Society: Washington, DC, 1989; p 166.
(66) Becke, A. D. *Int. J. Quantum Chem., Symp.* **1989**, *23*, 599.
(67) Perdew, J. P. *Phys. Rev. B* **1986**, *33*, 8822.

Supporting Information Available: Unit cell diagrams for $[N(CH_3)_4][OsO_4F]$ (Figure S6) and $[N(CH_3)_4][OsO_3F_3]$ (Figure S7), factor group analyses for the anions and cations in $[N(CH_3)_4][OsO_4F]$ (Table S8) and $[N(CH_3)_4][OsO_3F_3]$ (Table S9), and X-ray crystallographic files, in CIF format, for the structure determinations of $[N(CH_3)_4][OsO_4F]$ and $[N(CH_3)_4][OsO_3F_3]$. This material is available free of charge via the Internet at http://pubs.acs.org.

IC000259I